

1 **The Positive Effect of Formaldehyde on the Photocatalytic**

2 **Renoxification of Nitrate on TiO₂ Particles**

3
4 Yuhan Liu, Xuejiao Wang, Mengshuang Sheng, Chunxiang Ye, Jing Shang*

5 *State Key Joint Laboratory of Environmental Simulation and Pollution Control,*

6 *College of Environmental Sciences and Engineering, Peking University, 5 Yiheyuan*

7 *Road, Beijing 100871, P. R. China*

8
9 Corresponding author: Jing Shang

10 Email: shangjing@pku.edu.cn

11
12 **Abstract**

13 Renoxification is the process of recycling of NO₃⁻/HNO₃ into NO_x under
14 illumination, which is mostly ascribed to the photolysis of nitrate. TiO₂, a typical
15 mineral dust component, can play its photocatalytic role in “renoxification” process
16 due to NO₃ radical formed, and we define this process as “photocatalytic
17 renoxification”. Formaldehyde (HCHO), the most abundant carbonyl compound in
18 the atmosphere, may participate in the renoxification of nitrate-doped TiO₂ particles.
19 In this study, we established an environmental chamber reaction system with the
20 presence of HCHO and nitrate-doped TiO₂. The direct photolyses of both nitrate and
21 NO₃ radical were excluded by adjusting the illumination wavelength, so as to explore
22 the effect of HCHO on the “photocatalytic renoxification”. It is found that NO_x

23 concentration can reach up to more than 100 ppb for nitrate-doped TiO₂ particles,
24 while almost no NO_x was generated in the absence of HCHO. Nitrate type, relative
25 humidity and HCHO concentration were found to influence NO_x release. Adsorbed
26 HCHO may react with nitrate radicals through hydrogen abstraction to form adsorbed
27 HNO₃ on the surface, which is responsible for the release of NO_x. The mass
28 generation of NO_x was suggested to via the NO₃⁻-NO₃[·]-HCHO-HNO₃-NO_x pathway,
29 with HCHO and TiO₂ exhibiting a significant synergistic effect. Our proposed
30 reaction mechanism by which HCHO promotes photocatalytic renoxification is
31 helpful for deeply understanding the atmospheric photochemical processes and
32 nitrogen cycling.

33 **1 Introduction**

34 The levels of ozone (O₃) and hydroxyl radicals (\cdot OH) in the troposphere can be
35 promoted by nitrogen oxides (NO_x = NO + NO₂), such that NO_x plays an important
36 role in the formation of secondary aerosols and atmospheric oxidants (Platt et al.,
37 1980; Stemmler et al., 2006; Harris et al., 1982; Finlayson-Pitts and Pitts, 1999). NO_x
38 can be converted into nitric acid (HNO₃) and nitrate (NO₃⁻) through a series of
39 oxidation and hydrolysis reactions and is eventually removed from the atmosphere
40 through subsequent wet or dry deposition (Dentener and Crutzen, 1993; Goodman et
41 al., 2001; Monge et al., 2010; Bedjanian and El Zein, 2012). However, comparisons
42 of observations and modeling results for the marine boundary layer, land, and free
43 troposphere (Read et al., 2008; Lee et al., 2009; Seltzer et al., 2015) have shown
44 underestimation of HNO₃ or NO₃⁻ content, NO_x abundance, and NO_x/HNO₃ ratios,

45 indicating the presence of a new, rapid NO_x circulation pathway (Ye et al., 2016b;
46 Reed et al., 2017). Some researchers have suggested that deposited NO₃⁻ and HNO₃
47 can be recycled back to gas phase NO_x under illumination, via the renoxification
48 process (Schuttlefield et al., 2008; Romer et al., 2018; Bao et al., 2020; Shi et al.,
49 2021). Photolytic renoxification occurs under light with a wavelength of < 350 nm,
50 through the photolysis of NO₃⁻/HNO₃ adsorbed on the solid surface to generate NO_x.
51 Notably, the photolysis of NO₃⁻/HNO₃ is reported to occur at least 2 orders of
52 magnitude faster on different solid surfaces (natural or artificial) or aerosols than in
53 the gas phase (Ye et al., 2016a; Zhou et al., 2003; Baergen and Donaldson, 2013).
54 Several recent studies have shown that renoxification has important atmospheric
55 significance (Deng et al., 2010; Kasibhatla et al., 2018; Romer et al., 2018; Alexander
56 et al., 2020), providing the atmosphere with a new source of photochemically reactive
57 nitrogen species, i.e., HONO or NO_x, resulting in the production of more
58 photooxidants such as O₃ or ·OH (Ye et al., 2017), which further oxidize volatile
59 organic compounds (VOCs), leading to the formation of more chromophores, thereby
60 affecting the photochemical process (Bao et al., 2020).

61 Renoxification processes have recently been observed on different types of
62 atmospheric particles, such as urban grime and mineral dust (Ninneman et al., 2020;
63 Bao et al., 2018; Baergen and Donaldson, 2013; Ndour et al., 2009). Atmospheric
64 titanium dioxide (TiO₂) is mainly derived from windblown mineral dust, with mass
65 mixing ratios ranging from 0.1 to 10% (Chen et al., 2012). TiO₂ is widely used in
66 industrial processes and building exteriors for its favorable physical and chemical

67 properties. Titanium and nitrate ions have been found to coexist in atmospheric
68 particulates in different regions worldwide (Sun et al., 2005; Schwartz-Narbonne et al.,
69 2019). The relative content of TiO_2 and NO_3^- in atmospheric particles varies greatly,
70 and nitrate-coated TiO_2 (NO_3^- - TiO_2) aerosols containing TiO_2 as the main body can
71 be used to effectively represent particles for sandstorm modeling (Sun et al., 2005;
72 Kim et al., 2012). TiO_2 is a semiconductor metal oxide that can facilitate the
73 photolysis of nitrate and the release of NO_x due to its photocatalytic activity (Ndour et
74 al., 2009; Chen et al., 2012; Verbruggen, 2015; Schwartz-Narbonne et al., 2019).
75 Under ultraviolet (UV) light, TiO_2 generates electron-hole pairs in the conduction and
76 valence bands, respectively (Linsebigler et al., 1995). Nitrate ions adsorbed at the
77 oxide surface react with the photogenerated holes (h^+) to form nitrate radicals (NO_3^\cdot),
78 which are subsequently photolyzed to NO_x , mainly under visible light illumination
79 (Schuttlefield et al., 2008; George et al., 2015; Schwartz-Narbonne et al., 2019). Thus,
80 the renoxification of NO_3^- is faster on TiO_2 than on other oxides in mineral dust
81 aerosols such as SiO_2 or Al_2O_3 (Lesko et al., 2015; Ma et al., 2021). In this study, we
82 refer to renoxification involving h^+ and NO_3^- in the reaction as photocatalytic
83 renoxification based on the photocatalytic properties of TiO_2 .

84 Many previous studies have focused mainly on particulate nitrate- NO_x
85 photochemical cycling reactions, despite the potential impact of other reactant gases
86 in the atmosphere. Formaldehyde (HCHO), the most abundant carbonyl compound in
87 the atmosphere, which can react at night with NO_3^\cdot via hydrogen abstraction reactions
88 to form HNO_3 (Atkinson, 1991). Our previous study showed that the degradation rate

89 of HCHO was faster on NO_3^- - TiO_2 aerosols than on TiO_2 particles, perhaps as a result
90 of HCHO oxidation by $\text{NO}_3\cdot$ (Shang et al., 2017). To date, no studies have reported the
91 effect of HCHO on photocatalytic renoxification. Adsorbed HCHO would react with
92 $\text{NO}_3\cdot$ generated on the NO_3^- - TiO_2 aerosol surface, thus alter the surface nitrogenous
93 species and renoxification process. The present study is the first to explore the
94 combined effect of HCHO and photocatalytic TiO_2 particles on the renoxification of
95 nitrate. The wavelengths of the light sources were adjusted to exclude photolytic
96 renoxification while making photocatalytic renoxification available for better
97 elucidate the reaction mechanism. We investigated the effects of various influential
98 factors including nitrate type, nitrate content, RH, and initial HCHO concentration, to
99 understand the atmospheric renoxification of nitrate in greater detail.

100 **2 Methods**

101 **2.1 Environmental chamber setup**

102 Details of the experimental apparatus and protocol used in the current study have
103 been previously described (Shang et al., 2017). Briefly, the main body of the
104 environmental chamber is a 400 L polyvinyl fluoride (PVF) bag filled with synthetic
105 air (high purity N_2 (99.999%) mixed with high purity O_2 (99.999%) in the ratio of
106 79:21 by volume, Beijing Huatong Jingke Gas Chemical Co.). The chamber is
107 capable of temperature (~ 293 K) and relative humidity (0.8–70%) control using a
108 water bubbler and air conditioners, respectively. The chamber is equipped with two
109 light sources both with the central wavelength of 365 nm. One is a set of 36 W tube
110 lamps with a main spectrum of 320–400 nm and a small amount of 480–600 nm

111 visible light (Figure S1a). The other is a set of 12 W Light-emitting diode (LED)
112 lamps with a narrow main spectrum of 350-390 nm (Figure S1b). The light intensities
113 for the tube and LED lamp at 365 nm were $300 \mu\text{W}\cdot\text{cm}^{-2}$ and $200 \mu\text{W}\cdot\text{cm}^{-2}$,
114 respectively, measured in the middle of the chamber. NO_x concentrations at the outlet
115 of the chamber were monitored by a chemiluminescence NO_x analyzer (ECOTECH,
116 EC9841B). HCHO was generated by thermolysis of paraformaldehyde at 70°C and
117 detected via acetyl acetone spectrophotometric method using a UV-Vis
118 spectrophotometer (PERSEE, T6) or a fluorescence spectrophotometer (THERMO,
119 Lumina), depending on different initial HCHO concentrations. The particle size
120 distribution was measured by a Scanning Nano Particle Spectrometer (HCT,
121 SNPS-20). Electron Spin Resonance (Nuohai Life Science, MiniScope MS 5000) was
122 used to measure $\cdot\text{OH}$ on the surface of particles. 5,5-dimethyl-1-pyrroline-N-oxide
123 (DPMO, Enzo) was used as the capture agent. $50 \mu\text{L}$ particle-containing suspension
124 mixed with $50 \mu\text{L}$ DMPO (concentration of $200 \mu\text{M}$) was loaded in a 1 mm capillary.
125 Four 365 nm LED lamps were placed side by side vertically at a distance of about 1
126 cm from the capillary, and the measurement was carried out after 1 min of irradiation.
127 The modulation frequency was 100 kHz, the modulation amplitude was 0.2 mT, the
128 microwave power was 10 mW and the sweep time was 60 s.

129 **2.2 Nitrate- TiO_2 composite samples**

130 In our experiments, two nitrate salts, potassium nitrate (AR, Beijing Chemical
131 Works Co., Ltd) or ammonium nitrate (AR, Beijing Chemical Works Co., Ltd), were
132 complexed with pure TiO_2 ($\geq 99.5\%$, Degussa AG) powder or TiO_2 (1 wt.%) / SiO_2

133 mixed powder to prepare NO_3^- - TiO_2 or NO_3^- - TiO_2 (1 wt.%)/ SiO_2 samples. 250 mg
134 TiO_2 was simply mixed in nitrate solutions at the desired mass mixing ratio (with
135 nitrate content of 4 wt.%) to obtain a mash. The mash was dried at 90 °C and then
136 ground carefully for 30 min. A series of samples with different amount of nitrate were
137 prepared and diffuse reflectance fourier transform infrared spectroscopy (DRIFTS)
138 measurements were made to test their homogeneity. Figure S2 shows DRIFTS spectra
139 of these KNO_3 - TiO_2 composites, of which 1760 cm^{-1} peak is one of the typical
140 vibrating peaks of nitrate (Aghazadeh, 2016; Maeda et al., 2011). Ratio value of peak
141 area from 1730 - 1790 cm^{-1} for 1, 4, 32, 80 wt.% composited samples is 1: 4.1: 29.8:
142 81.6, which is very close to that of theoretical value, proving that the samples were
143 uniformly mixed. SiO_2 (AR, Xilong Scientific Co., Ltd.) with no optical activity was
144 also chosen for comparison, and samples of KNO_3 - SiO_2 and KNO_3 - TiO_2 (1
145 wt.%)/ SiO_2 samples with a potassium nitrate content of 4 wt.% were prepared. The
146 blank 250 mg TiO_2 sample was solved in pure water with the same procedure as
147 mentioned above. 4 wt.% HNO_3 - TiO_2 composite particles were prepared for
148 comparison. Concentrated nitric acid (AR, Beijing Chemical Works Co., Ltd) was
149 diluted to 1 M and 250 mg TiO_2 was added to the nitric acid solution and stirred
150 evenly. A layer of aluminum foil was covered on the surface of the HNO_3 - TiO_2
151 homogenate and dried naturally in the room and then ground for use. We also selected
152 Arizona Test Dust (ATD, Powder Technology Inc.), whose chemical composition and
153 weight percentage were shown in Table S1, as a substitute of NO_3^- / TiO_2 to investigate
154 the “photocatalytic renoxification” process of nitrate and the positive effect of HCHO.

155 **2.3 Environmental chamber experiments**

156 For the chamber operation, we completely evacuated the chamber after every
157 experiment, then cleaned the chamber walls with deionized water and then dried by
158 flushing the chamber with ultra-zero air to remove any particles or gases collected on
159 the chamber walls. The experiments carried out in the environmental chamber can be
160 divided into two categories according to whether HCHO was involved or not. (1) No
161 HCHO involvement in the reaction. The PVF bag was inflated by 260 L synthetic air,
162 and then 75 mg particles were instantly sprayed into the chamber by a transient
163 high-pressure airflow. As shown in Figure S3, the particle number concentration of
164 KNO₃-TiO₂ or TiO₂ sample decreased rapidly owing to wall effect including the
165 possible electrostatic adsorption of the particles by the environmental chamber. The
166 size distributions of KNO₃-TiO₂ and TiO₂ samples were similar, with both reached
167 stable after about 60 min. The peak number concentration was averaged of 3991 and
168 3886 particle/cm⁻³ during illumination period for KNO₃-TiO₂ and TiO₂ sample,
169 respectively, indicating that the repeatability of the introduction of particles into the
170 chamber is good. This can be attributed to the strict cleaning of the chamber and the
171 same operation of each batch experiment. (2) With the participation of HCHO. The
172 PVF bag was inflated by 125 L synthetic air, followed by the introduction of HCHO,
173 and then the chamber was filled up with zero air to about 250 L. In order to know the
174 HCHO adsorption before and after the particles' introduction, we conducted a
175 conditional experiment in the dark. It can be seen from Figure S4 that it took about 90
176 min for the concentration of HCHO to reach stable, and can be sustained. Then, 75

177 mg TiO_2 or $\text{NO}_3^-/\text{TiO}_2$ powders were introduced instantly and the concentration of
178 HCHO decreased upon the introduction. It took about 60 min for HCHO to reach its
179 second adsorption equilibrium, and the concentration of HCHO can be stable for
180 several hours in the dark. Therefore, for the irradiation experiments, the particles were
181 injected at 90 min after HCHO's introduction, and the lamps were turned on at 60 min
182 after the particle's introduction.

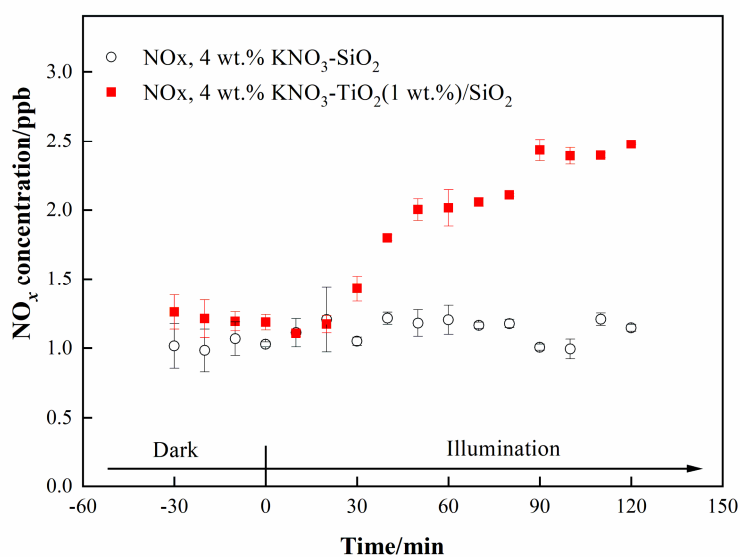
183 To determine the background value of NO_x in the reaction system, four blank
184 experiments were carried out under illumination without nitrate: "synthetic air",
185 "synthetic air + TiO_2 ", "synthetic air + HCHO" and "synthetic air + HCHO + TiO_2 ".
186 In the blank experiments of "synthetic air" and "synthetic air + TiO_2 ", the NO_x
187 concentration remained stable during 180 min illumination, and the concentration
188 change was no more than 0.5 ppb (Figure S5a). Therefore, the environmental chamber,
189 synthetic air and the surface of TiO_2 particles were thought to be relatively clean, and
190 there was no generation and accumulation of NO_x under illumination. When HCHO
191 was introduced into the environmental chamber, NO_x accumulated ~2 ppb in 120 min
192 with or without TiO_2 particles (Figure S5b). Compared with the blank experiment
193 results when there was no HCHO, NO_x might come from the generation process of
194 HCHO (impurities in paraformaldehyde). However, considering the high
195 concentration level of NO_x produced in the NO_3^- - TiO_2 system containing HCHO
196 under the same conditions in this study (see later in Figure 2), the NO_x generated in
197 this blank experiment can be negligible.

198

199 **3 Results and discussion**

200 **3.1 The positive effect of TiO₂ on the renoxification process**

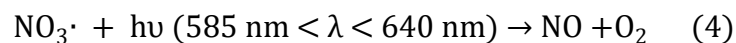
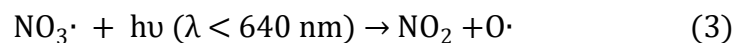
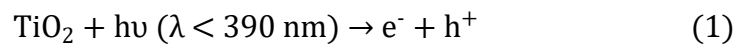
201 We investigated the photocatalytic role of TiO₂ on renoxification. The light
202 source was two 365 nm tube lamps containing small amounts of 400–600 nm visible
203 light; this setup was suitable for exciting TiO₂ and the photolysis of available nitrate
204 radicals. Raw NO_x data measured in the chamber under dark and illuminated
205 conditions for 4 wt.% KNO₃-SiO₂ and 4 wt.% KNO₃-TiO₂ (1 wt.%)/SiO₂ are shown
206 in Figure 1. The ratio of 1 wt. % TiO₂ to SiO₂ corresponds to their ratio in sand and
207 dust particles. We observed no NO_x in the KNO₃-SiO₂ sample under dark or
208 illumination, indicating very weak direct photolysis of nitrate under our 365 nm
209 tube-lamp illumination conditions. However, when the sample containing TiO₂/SiO₂
210 was illuminated, NO_x continually accumulated in the chamber. This finding confirms
211 that NO_x production arising from photodissociation of NO₃⁻ on TiO₂/SiO₂ was caused
212 by the photocatalytic property of TiO₂ (i.e., photocatalytic renoxification) and was not
213 due to the direct photolysis of NO₃⁻ (photolytic renoxification).



214

215 **Figure 1.** Effect of illumination on the release of NO_x from 4 wt.% KNO₃-SiO₂ and 4
216 wt.% KNO₃-TiO₂(1 wt.%)/SiO₂ at 293 K and 0.8% of relative humidity. 365 nm tube
217 lamps were used during the illumination experiments.

218 TiO₂ can be excited by UV illumination to generate electron-hole pairs, and the
219 h⁺ can react with adsorbed NO₃⁻ to produce NO₃[·] (Ndour et al., 2009). Thus, in the
220 present study, NO₃[·] mainly absorbed visible light emitted from the tube lamps, which
221 was subsequently photolyzed to NO_x through Eqs. (3) and (4) (Wayne et al., 1991),
222 which explains why NO_x was observed in this study. Thus, we demonstrated that TiO₂
223 can be excited at illumination wavelengths of ~365 nm, even when then content was
224 very low, and that NO_x accumulated due to the production and further phytolysis of
225 NO₃[·]. However, the production rate of NO_x was very slow, reaching only 1.3 ppb
226 during 90 min of illumination. This result may have been caused by the blocking
227 effect of K⁺ on NO₃⁻. K⁺ forms ion pairs with NO₃⁻, and electrostatic repulsion
228 between K⁺ and h⁺ prevents NO₃⁻ from combining with h⁺ to generate NO₃[·] to a
229 certain extent, thereby weakening the positive effect of TiO₂ on the renoxification of
230 KNO₃ (Rosseler et al., 2013).



231

232

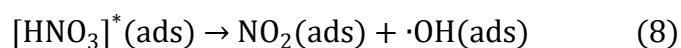
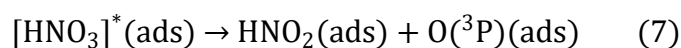
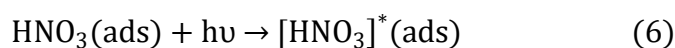
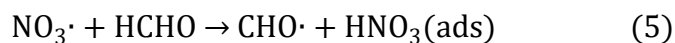
233 **3.2 The synergistic positive effect of TiO₂ and HCHO on the renoxification**
234 **process**

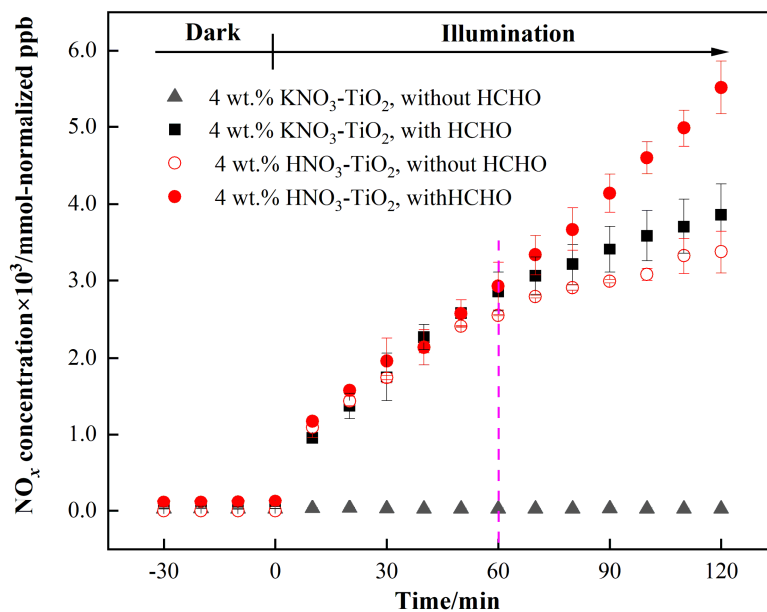
235 LED lamps with a wavelength range of 350–390 nm and no visible light were
236 used to irradiate 4 wt.% KNO₃-TiO₂ without generating NO_x (NO₂ and NO
237 concentrations fluctuate within the error range of the instrument) (Figure S5). TiO₂
238 can be excited under this range of irradiation, producing NO₃ radicals as discussed
239 above. The lack of NO_x generation indicates that neither nitrate photolysis nor
240 NO₃· photolysis occurred under 365 nm LED lamp illumination conditions. In
241 addition, it has been shown that NO₃· photolysis only occurs in visible light (Aldener
242 et al., 2006). Therefore, the LED lamp setup was used in subsequent experiments to
243 exclude the direct photolysis of both KNO₃ and NO₃·, but allow the excitation of TiO₂.
244 This approach allowed us to investigate the process of photocatalytic renoxification
245 caused by HCHO in the presence of photogenerated NO₃·.

246 Atmospheric trace gases can undergo photocatalytic reactions on the surface of
247 TiO₂ (Chen et al., 2012). As the illumination time increased, the concentration of
248 HCHO showed a linear downward trend, which was found to fit zero-order reaction
249 kinetics (Figure S7). The zero-order reaction rate constants of HCHO on TiO₂ and 4
250 wt.% KNO₃-TiO₂ particles were 9.1×10^{-3} and 1.4×10^{-2} ppm min⁻¹, respectively,
251 which were much higher than that for gaseous HCHO photolysis (Shang et al., 2017).
252 We suggested that the produced NO₃· contributed to the enhanced uptake of HCHO.
253 In the following study, the effect of HCHO on the photocatalytic renoxification of
254 NO₃⁻-TiO₂ was explored.

255 Variation in NO_x concentration within the chamber containing nitrate- TiO_2
256 particles with or without HCHO is shown in Figure 2. For 4 wt.% KNO_3 - TiO_2
257 particles, the NO_x concentration began to increase upon irradiation in the presence of
258 HCHO, reaching ~ 3861 mmol-normalized ppb (equivalent to 110 ppb) within 120
259 min. This result indicates that HCHO greatly promoted photocatalytic renoxification
260 of KNO_3 on the surfaces of TiO_2 particles. This reaction process can be divided into
261 two stages: a rapid increase within the first 60 min and a slower increase within the
262 following 60 min, each consistent with zero-order reaction kinetics. The slow stage is
263 due to the photodegradation of HCHO on KNO_3 - TiO_2 aerosols, which led to a
264 decrease in its concentration, gradually weakening the positive effect. NO_x is the sum
265 of NO_2 and NO , both of which showed a two-stage concentration increase (Figure S8).
266 The NO_2 generation rate was nearly 6 times that of NO , as compared to using the
267 zero-order rate constant within 60 min ($1.18 \text{ ppb min}^{-1} \text{ NO}_2$, $R^2 = 0.96$; 0.19 ppb
268 $\text{min}^{-1} \text{ NO}$, $R^2 = 0.91$). This burst-like generation of NO_x can be ascribed to the
269 reaction between generated $\text{NO}_3\cdot$ and HCHO via hydrogen abstraction to form
270 adsorbed nitric acid ($\text{HNO}_3(\text{ads})$) on TiO_2 particles. We measured the pH of water
271 extracts in NO_3^- - TiO_2 systems with and without HCHO. It was found that the pH
272 decreased by 1.7% for KNO_3 - TiO_2 , suggesting the formation of acidic species such as
273 $\text{HNO}_3(\text{ads})$ in this study. Based on the analysis of the absorption cross section of
274 HNO_3 adsorbed on fused silica surface, the $\text{HNO}_3(\text{ads})$ absorption spectrum has been
275 reported to be red-shifted compared to $\text{HNO}_3(\text{g})$, extending from 350 to 365 nm, with
276 a simultaneous cross-sectional increase (Du and Zhu, 2011). Therefore, $\text{HNO}_3(\text{ads})$

277 was subjected to photolysis to produce NO₂ and HONO (Eqs. (6)-(8)) under the LED
278 lamp used in this study. A previous study of HNO₃ photolysis on the surface of Pyrex
279 glass showed that the ratio of the formation rates of photolysis products
280 ($J_{\text{NO}_x}/J_{(\text{NO}_x+\text{HONO})}$) was > 97% at RH = 0% (Zhou et al., 2003), suggesting that NO_x is
281 the main gaseous product under dry conditions. Thus, the effect of HONO on product
282 distribution and NO_x concentration was negligible in this study. Together, these results
283 suggest that NO₃· and HCHO generate HNO₃(ads) on particle surfaces through
284 hydrogen abstraction, which contributes to the substantial release of NO_x via
285 photolysis. This photocatalytic renoxification via the NO₃⁻-NO₃·-HCHO-HNO₃-NO_x
286 pathway is important considering the high abundance of hydrogen donor organics in
287 the atmosphere.





288

289 **Figure 2.** Effect of formaldehyde on the renoxification processes of different nitrate-
 290 doped particles at 293 K and 0.8% of relative humidity. 365 nm LED lamps were used
 291 during the illumination experiment. The initial concentration of HCHO was about 9
 292 ppm.

293 To demonstrate the proposed HCHO mechanism and the photolysis contribution
 294 of HNO₃ to NO_x, we prepared an HNO₃-TiO₂ sample by directly dissolving TiO₂ into
 295 dilute nitric acid. The formation of NO_x on HNO₃-TiO₂ without HCHO under
 296 illumination was obvious and at a rate comparable with, that on KNO₃-TiO₂ with
 297 HCHO (Figure 2). The renoxification of HNO₃-TiO₂ particles was further enhanced
 298 following the introduction of HCHO. This is because that HNO₃ dissociates on
 299 particle surfaces to generate NO₃⁻, such that HNO₃ exists on TiO₂ as both HNO₃(ads)
 300 and NO₃⁻(ads). Similarly, NO₃⁻(ads) completed the NO₃⁻-NO₃·-HCHO-HNO₃-NO_x
 301 pathway as described above through the reaction process shown in Eqs. (2) to (8). The
 302 rates of NO_x production from HNO₃-TiO₂ particles with and without HCHO were

303 similar for the first 60 min (Figure 2), mainly due to the direct photolysis of partial
304 HNO₃(ads). However, after 60 min, NO_x was generated rapidly in the presence of
305 HCHO, perhaps due to the dominant photocatalytic renoxification of NO₃⁻(ads).
306 These findings indicate that HCHO converts NO₃⁻ on particle surfaces into HNO₃(ads)
307 by reacting with NO₃[·], and then HNO₃(ads) photolyzes at a faster rate to generate
308 NO_x, allowing HCHO to enhance the formation of NO_x. Overall, the photocatalytic
309 renoxification of NO₃⁻-TiO₂ particles affects atmospheric oxidation and the nitrogen
310 cycle, and the presence of HCHO further enhances this impact.

311 Photocatalytic renoxification reaction occurs on the surfaces of mineral dust due
312 to the presence of semiconductor oxides with photocatalytic activity such as TiO₂
313 (Ndour et al., 2009). In order to confirm this, we synthesized nitrate with inert SiO₂ as
314 a comparison. It can be seen from Figure S9 that no NO₂ formation was observed
315 whether HCHO was present or not, indicating that photocatalytically active particle
316 TiO₂ is critical to the photocatalytic renoxification process. Furthermore, a kind of
317 commercial mineral dust ATD was selected to study the effects of HCHO on this
318 process. We detected ·OH in irradiated pure TiO₂ and ATD samples using electron
319 spin resonance (ESR) technique, and found that for ATD samples, the peak intensity
320 of ·OH generation was 40% that of TiO₂ samples (Figure S10). ·OH originates in the
321 reaction of h⁺ with surface adsorbed water (Ahmed et al., 2014). ATD contains
322 semiconductor oxides such as TiO₂ and Fe₂O₃, and is thought to exhibit photocatalytic
323 properties affecting the renoxification of nitrate. The NO₃⁻ content of ATD is 4 × 10¹⁷
324 molecules m⁻², which is ~0.25 wt.% of the total mass (Huang et al., 2015; Jiyeon et

325 al., 2017). The NO_x concentration changes observed in the environmental chamber
326 demonstrated that HCHO promoted the renoxification of ATD particles (Figure S11).
327 This result suggests that mineral dust containing photocatalytic semiconductor oxides
328 such as TiO_2 , Fe_2O_3 , and ZnO can greatly promote the conversion of granular nitrate
329 to NO_x in the presence of HCHO.

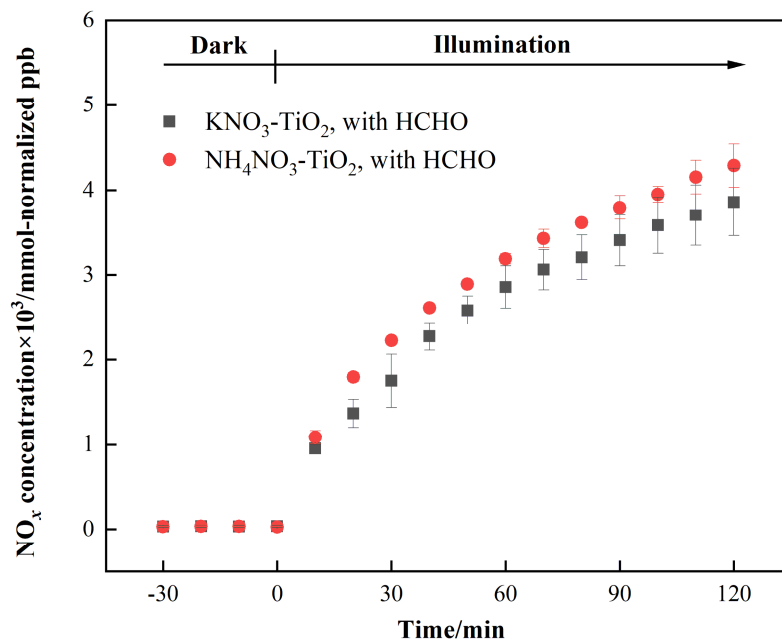
330 **3.3 Influential factors on the photocatalytic renoxification process**

331 **3.3.1 The influence of nitrate type**

332 As discussed above, HNO_3 and KNO_3 undergo different renoxification processes
333 on the surface of TiO_2 under the same illumination conditions, suggesting that cations
334 bound to NO_3^- significantly affect NO_x production. Different types of cations coexist
335 with nitrate ions in atmospheric particulate matter, among which ammonium ions
336 (NH_4^+) are important water-soluble ions that can be higher in content than K^+ in urban
337 fine particulate matter (Zhou et al., 2016; Tang et al., 2021; Wang et al., 2021),
338 especially in heavily polluted cities.(Tian et al., 2020) Equal amounts of 4 wt.%
339 $\text{NH}_4\text{NO}_3\text{-TiO}_2$ particles were introduced into the chamber and illuminated under the
340 same conditions. Similar as Figure 2, millimole normalized ppb was used in order to
341 compare the amount of NO_x release for different kinds of nitrate with same percentage
342 weight. It can be seen that HCHO had a much stronger positive effect on the release
343 of NO_x over $\text{NH}_4\text{NO}_3\text{-TiO}_2$ particles (Figure 3), which may be ascribed to NH_4^+ .
344 Combined with the results of $\text{NH}_4\text{NO}_3\text{-TiO}_2$ and $\text{KNO}_3\text{-TiO}_2$ particles, it seems that
345 the affinity rather than electrostatic repulsion should be the primary effect of cations
346 on the production of NO_x . On substrates without photocatalytic activity such as SiO_2

347 and Al₂O₃, NH₄NO₃ cannot generate NO_x,(Ma et al., 2021) such that NO_x production
348 depends on the effect of TiO₂. The h⁺ generated by TiO₂ excitation reacts with
349 adsorbed H₂O to produce ·OH (Eq. (9)), which gradually oxidizes NH₄⁺ to NO₃⁻ (Eq.
350 (10)). In our previous study, we demonstrated that irradiated (NH₄)₂SO₄-TiO₂ samples
351 had lower NH₄⁺ and NO₃⁻ peaks (Shang et al., 2017). Therefore, more NO₃⁻
352 participated in the photocatalytic renoxification process via the
353 NO₃⁻-NO₃[·]-HCHO-HNO₃-NO_x pathway to generate NO_x. Moreover , the results
354 without HCHO are shown in Figure S12, both NH₄NO₃-TiO₂ particles and
355 KNO₃-TiO₂ particles produced almost no NO_x, indicating the importance of HCHO
356 for renoxification to occur. Due to the high content of NH₄NO₃ in atmospheric
357 particulate matter, the positive effect of HCHO on the photocatalytic renoxification
358 process may have some impact on the concentrations of NO_x and other atmospheric
359 oxidants.





361

362 **Figure 3.** Effect of formaldehyde on the renoxification processes of 4 wt.%

363 NH₄NO₃-TiO₂ and 4 wt.% KNO₃-TiO₂ particles at 293 K and 0.8% of relative

364 humidity. 365 nm LED lamps were used during the irradiation experiment. The initial

365 concentration of HCHO was about 9 ppm.

366

367 3.3.2 The influence of relative humidity

368 Water on particle surfaces can participate directly in the heterogeneous reaction

369 process. As shown in Eq. (9), H₂O can be captured by h⁺ to generate ·OH with strong

370 oxidizability in photocatalytic reactions. The first-order photolysis rate constant of

371 NO₃⁻ on TiO₂ particles decreases by an order of magnitude, from $(5.7 \pm 0.1) \times 10^{-4} \text{ s}^{-1}$

372 on dry surfaces to $(7.1 \pm 0.8) \times 10^{-5} \text{ s}^{-1}$ when nitrate is coadsorbed with water above

373 monolayer coverage (Ostaszewski et al., 2018). We explored the positive effect of

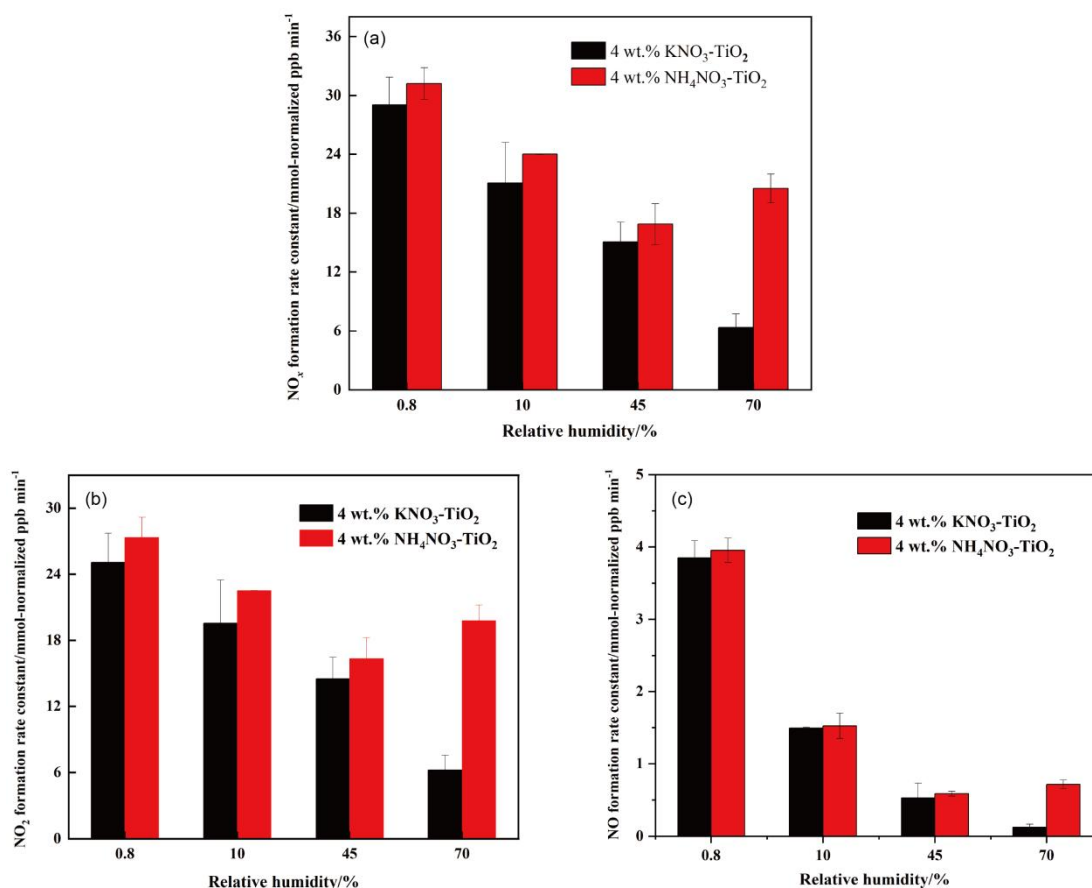
374 HCHO on the NO₃⁻-TiO₂ particle photocatalytic renoxification at different RH levels;

375 the results are shown in Figure 4a. For KNO₃-TiO₂ particles, the rate of NO_x

376 production decreased as the RH of the environmental chamber increased, indicating
377 that increased water content in the gas phase hindered photocatalytic renoxification
378 for two reasons: H₂O competes with NO₃⁻ for h⁺ on the surface of TiO₂ to
379 generate ·OH, reducing the generation of NO₃·, and competitive adsorption between
380 H₂O and HCHO causes the generated ·OH to compete with NO₃· for HCHO,
381 hindering the formation of HNO₃(ads) on particle surfaces. Moreover, it is also
382 possible that the loss of NO_x on the wall increases under high humidity conditions,
383 resulting in a decrease in its concentration. This competitive process also occurs on
384 the surface of NH₄NO₃-TiO₂ particles, but at RH = 70%, the NO_x generation rate
385 constant is slightly higher. The deliquescent humidity of NH₄NO₃ at 298 K is ~62%,
386 such that NH₄NO₃ had already deliquesced at RH = 70%, forming an NH₄⁺/NH₃-NO₃⁻
387 liquid system on the particle surfaces. This quasi-liquid phase improved the dispersion
388 of TiO₂ in NH₄NO₃, resulting in greater NO_x release. The deliquescent humidity of
389 KNO₃-TiO₂ was > 90%,(2009) such that no phase change occurred at RH = 70%, and
390 the renoxification reaction rate retained a downward trend. In the presence of H₂O, in
391 addition to the NO₃⁻-NO₃·-HCHO-HNO₃ pathway observed in this study, there are a
392 variety of HNO₃ generation paths, such as the hydrolysis of N₂O₅ via the
393 NO₂-N₂O₅-HNO₃ pathway (Brown et al., 2005), the oxidation of NO₂ by ·OH
394 (Burkholder et al., 1993), and the reaction of NO₃· with H₂O (Schutze and Herrmann,
395 2005), all of which require further consideration and study.

396 The formation rates of NO and NO₂ are shown in Figure 4b and c, respectively.
397 NO₂ was the main product of surface HNO₃ photolysis. Under humid conditions,

398 generated $\text{NO}_2(\text{ads})$ continued to react with H_2O adsorbed on the surface to form
399 $\text{HONO}(\text{ads})$. HONO was desorbed from the surface and released into the gas phase
400 (Zhou et al., 2003; Bao et al., 2018; Pandit et al., 2021), providing gaseous HONO to
401 the reaction system. Because the NO_x concentration remained high, the effect of
402 HONO on NO_x analyzer results was negligible (Shi et al., 2021). As NO_2 can form
403 NO_2^- with e^- , a reverse reaction also occurred between NO_2^- and HONO in the
404 presence of H_2O (Ma et al., 2021; Garcia et al., 2021). Therefore, the increase in H_2O
405 increased the proportion of HONO in the nitrogen-containing products, such that the
406 NO_x generation rate decreased as RH increased. Comparing Figure 4b and c shows
407 that, as RH increased, the NO production rate constant decreased more than that of
408 NO_2 . HONO and NO_2 generated by the photolysis of $\text{HNO}_3(\text{ads})$ decreased
409 accordingly, i.e., the NO source decreased. However, generated NO_2 and NO
410 underwent photocatalytic oxidation on the surface of TiO_2 , and NO photodegradation
411 was more significant under the same conditions (Hot et al., 2017). Generally, a certain
412 amount of HONO will be generated during the reaction between HCHO and
413 NO_3^- - TiO_2 particles when RH is high, which affects the concentrations of
414 atmospheric $\cdot\text{OH}$, NO_x , and O_3 . This process is more likely to occur in summer due to
415 high RH and light intensity affecting atmospheric oxidation. In drier winters or dusty
416 weather, when TiO_2 content is high, HCHO greatly promotes the photocatalytic
417 renoxification of NO_3^- - TiO_2 particles, thereby releasing more NO_x into the atmosphere,
418 affecting the global atmospheric nitrogen budget. Thus, regardless of the seasonal and
419 regional changes, renoxification has significant practical importance.



420

421 **Figure 5.** Effect of relative humidity on the release of NO_x (a), NO₂ (b), NO (c) over 4

422 wt.% NH₄NO₃-TiO₂ and 4 wt.% KNO₃-TiO₂ particles at 293 K. 365 nm LED lamps

423 were used during the illumination experiment. The initial concentration of HCHO was

424 about 9 ppm.

425

426 3.3.3 The influence of initial HCHO concentration

427 To explore whether HCHO promotes nitrate renoxification at natural

428 concentration levels, we reduced the initial concentration of HCHO in the

429 environmental chamber by a factor of 10, to ~1.0 ppm. The positive effect of HCHO

430 on the photocatalytic renoxification of KNO₃-TiO₂ particles was clearly weakened,

431 with NO₂ concentration first increasing and then decreasing, and NO concentration

432 remaining stable (Figure S13). The HCHO concentration decreased due to its
433 consumption during the reaction, making its positive effect decline quickly. The
434 photocatalytic oxidation reaction between NO_x and photogenerated reactive oxygen
435 species (ROS) on the TiO_2 surface further decreased the NO_x concentration.
436 Photocatalytic oxidation of NO_x by ROS on TiO_2 particles occurred at an HCHO
437 concentration of 9 ppm, but the positive effect of HCHO remained dominant. Thus,
438 no decrease in NO_x concentration was observed within 120 min in our experiments.

439 The concentration of HCHO in the atmosphere is relatively low, with a balance
440 between the photocatalytic oxidation decay of NO_x and the release of NO_x via
441 photocatalytic renoxification. The mutual transformation between particulate NO_3^-
442 and gaseous NO_x is more complex. The effect of low-concentration HCHO on the
443 renoxification of NO_3^- - TiO_2 particles requires further investigation. However, many
444 types of organics provide hydrogen atoms in the atmosphere, including alkanes (e.g.,
445 methane and n-hexane), aldehydes (e.g., acetaldehyde), alcohols (e.g., methanol and
446 ethanol), and aromatic compounds (e.g., phenol) that react with $\text{NO}_3\cdot$ to produce nitric
447 acid (Atkinson, 1991). These organics, together with HCHO, play similar positive
448 roles in photocatalytic renoxification and, therefore, influence NO_x concentrations.

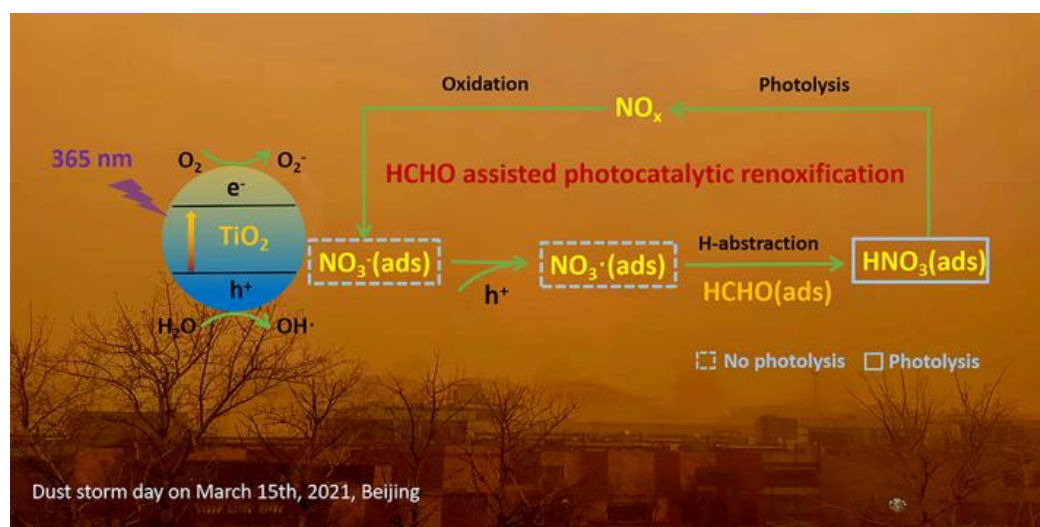
449

450 **4 Atmospheric implications**

451 Nitric acid and nitrate are not only the final sink of NO_x in the atmosphere but
452 are also among its important sources. NO_x from nitrate through renoxification is easily
453 overlooked. The renoxification of nitrate on the surface of TiO_2 particles can be

454 divided into photolytic renoxification and photocatalytic renoxification. The
455 photocatalytic performance of TiO₂ promotes the renoxification process, which
456 explains the influence of semiconducting metal oxide components on atmospheric
457 mineral particles during the renoxification of nitrate. Although most previous studies
458 have focused on solid-phase nitrate renoxification, our exploration of the roles of
459 HCHO in this study will allow us to examine complex real-world pollution scenarios,
460 in which multiple atmospheric pollutants coexist, as well as the effects of organic
461 pollutants on the renoxification process. Atmospheric HCHO is taken up at the
462 surface of particulate matter, accounting for up to ~50% of its absorption (Li et al.,
463 2014), such that the heterogeneous participation of HCHO during renoxification is
464 important. This study is the first to report that HCHO has a positive effect on the
465 photocatalytic renoxification of nitrate on TiO₂ particles, via the
466 NO₃⁻-NO₃[·]-HCHO-HNO₃-NO_x pathway (Figure 5), further increasing the release of
467 NO_x and other nitrogen-containing active species, which in turn affects the
468 photochemical cycle of HO_x radicals in the atmosphere and the formation of
469 important atmospheric oxidants such as O₃. Although in the case of high
470 concentrations of HCHO in our experiment, the response to the real situation will be
471 biased, the results of this study illustrate a possible way of HCHO in influencing
472 nitrate renoxification in the atmosphere. Factors such as particulate matter
473 composition, RH, and initial HCHO concentration all influence the positive effect of
474 HCHO; notably, H₂O competes with NO₃⁻ for photogenerated holes. Based on these
475 findings, two balance systems should be explored in depth: the influence of RH on the

476 generation rates of HONO and NO_x , as water increases the proportion of HONO in
 477 nitrogen-containing products; and the balance between the photocatalytic degradation
 478 of generated NO_x on TiO_2 particles and the positive effect of HCHO on NO_x
 479 generation at low HCHO concentrations.



480

481 **Figure 5.** Positive role of HCHO on the photocatalytic renoxification of nitrate- TiO_2
 482 composite particles via the NO_3^- - NO_3^+ -HCHO- HNO_3 - NO_x pathway.

483 Based on our results, we conclude that in photochemical processes on the
 484 surfaces of particles containing semiconductor oxides, with the participation of
 485 hydrogen donor organics, a significant synergistic photocatalytic renoxification
 486 enhancement effect alters the composition of surface nitrogenous species via the
 487 NO_3^- - NO_3^+ -hydrogen donor- HNO_3 - NO_x pathway, thereby affecting atmospheric
 488 oxidation and nitrogen cycling. The positive effect of HCHO can be extended from
 489 TiO_2 in this study to other components of mineral dust such as Fe_2O_3 and ZnO with
 490 photocatalytic activity, which may have practical applications. Our proposed reaction
 491 mechanism by which HCHO promotes photocatalytic renoxification will improve
 492 existing atmospheric chemistry models and reduce discrepancies between model

493 simulations and field observations.

494

495 ***Supplement.***

496 Detailed information of Figures S1-13 (which include the spectra of the lamps,
497 size distribution of 4 wt.% KNO₃-TiO₂ and TiO₂ particles and changes of HCHO
498 concentration in environmental chamber, changes of NO_x concentration under
499 different reaction conditions, photodegradation curve of HCHO, ESR spectra of TiO₂
500 and ATD particles), and Table S1 (which demonstrate ATD chemical composition) .

501

502 ***Acknowledgments***

503 The authors are grateful to the financial support provided by National Natural
504 Science Foundation of China (Nos. 21876003, 41961134034 and 21277004), the
505 Second Tibetan Plateau Scientific Expedition and Research (No. 2019QZKK0607).

506

507 **References**

508 Aghazadeh, M.: Preparation of Gd₂O₃ Ultrafine Nanoparticles by Pulse
509 Electrodeposition Followed by Heat-treatment Method, Journal of Ultrafine Grained
510 and Nanostructured Materials, 49, 80-86, 10.7508/jufgmsm.2016.02.04, 2016.

511 Ahmed, A. Y., Kandiel, T. A., Ivanova, I., and Bahnemann, D.: Photocatalytic and
512 photoelectrochemical oxidation mechanisms of methanol on TiO₂ in aqueous solution,
513 Applied Surface Science, 319, 44-49, 10.1016/j.apsusc.2014.07.134, 2014.

514 Aldener, M., Brown, S. S., Stark, H., Williams, E. J., Lerner, B. M., Kuster, W. C.,
515 Goldan, P. D., Quinn, P. K., Bates, T. S., Fehsenfeld, F. C., and Ravishankara, A. R.:
516 Reactivity and loss mechanisms of NO₃ and N₂O₅ in a polluted marine environment:
517 Results from in situ measurements during New England Air Quality Study 2002,

518 Journal of Geophysical Research-Atmospheres, 111, D23S73, 10.1029/2006jd007252,
519 2006.

520 Alexander, B., Sherwen, T., Holmes, C. D., Fisher, J. A., Chen, Q., Evans, M. J., and
521 Kasibhatla, P.: Global inorganic nitrate production mechanisms: comparison of a
522 global model with nitrate isotope observations, *Atmospheric Chemistry and Physics*,
523 20, 3859-3877, 10.5194/acp-20-3859-2020, 2020.

524 Atkinson, R.: Kinetics and mechanisms of the gas-phase reactions of the NO₃ radical
525 with organic-comounds, *Journal of Physical and Chemical Reference Data*, 20,
526 459-507, 10.1063/1.555887, 1991.

527 Baergen, A. M. and Donaldson, D. J.: Photochemical Renoxification of Nitric Acid on
528 Real Urban Grime, *Environmental Science & Technology*, 47, 815-820,
529 10.1021/es3037862, 2013.

530 Bao, F., Li, M., Zhang, Y., Chen, C., and Zhao, J.: Photochemical Aging of Beijing
531 Urban PM_{2.5}: HONO Production, *Environmental Science & Technology*, 52,
532 6309-6316, 10.1021/acs.est.8b00538, 2018.

533 Bao, F., Jiang, H., Zhang, Y., Li, M., Ye, C., Wang, W., Ge, M., Chen, C., and Zhao, J.:
534 The Key Role of Sulfate in the Photochemical Renoxification on Real PM_{2.5},
535 *Environmental Science & Technology*, 54, 3121-3128, 10.1021/acs.est.9b06764,
536 2020.

537 Bedjanian, Y. and El Zein, A.: Interaction of NO₂ with TiO₂ Surface Under UV
538 Irradiation: Products Study, *Journal of Physical Chemistry A*, 116, 1758-1764,
539 10.1021/jp210078b, 2012.

540 Brown, S. S., Osthoff, H. D., Stark, H., Dube, W. P., Ryerson, T. B., Warneke, C., de
541 Gouw, J. A., Wollny, A. G., Parrish, D. D., Fehsenfeld, F. C., and Ravishankara, A. R.:
542 Aircraft observations of daytime NO₃ and N₂O₅ and their implications for
543 tropospheric chemistry, *Journal of Photochemistry and Photobiology a-Chemistry*,
544 176, 270-278, 10.1016/j.jphotochem.2005.10.004, 2005.

545 Burkholder, J. B., Talukdar, R. K., Ravishankara, A. R., and Solomon, S.:
546 Temperature-dependence of the HNO₃ UV absorption cross-sections, *Journal of*
547 *Geophysical Research-Atmospheres*, 98, 22937-22948, 10.1029/93jd02178, 1993.

548 Chen, H., Nanayakkara, C. E., and Grassian, V. H.: Titanium Dioxide Photocatalysis
549 in Atmospheric Chemistry, *Chemical Reviews*, 112, 5919-5948, 10.1021/cr3002092,
550 2012.

551 Deng, J. J., Wang, T. J., Liu, L., and Jiang, F.: Modeling heterogeneous chemical
552 processes on aerosol surface, *Particuology*, 8, 308-318, 10.1016/j.partic.2009.12.003,
553 2010.

554 Dentener, F. J. and Crutzen, P. J.: Reaction of N_2O_5 on tropospheric aerosols-impact
555 on the global distributions of NO_x , O_3 , and OH, *Journal of Geophysical*
556 *Research-Atmospheres*, 98, 7149-7163, 10.1029/92jd02979, 1993.

557 Du, J. and Zhu, L.: Quantification of the absorption cross sections of surface-adsorbed
558 nitric acid in the 335-365 nm region by Brewster angle cavity ring-down spectroscopy,
559 *Chemical Physics Letters*, 511, 213-218, 10.1016/j.cplett.2011.06.062, 2011.

560 Finlayson-Pitts, B. J. and Pitts, J. J. N.: *Chemistry of the Upper and Lower*
561 *Atmosphere: Theory, Experiments and Applications*, 10.1023/A:1024719803484,
562 Academic Press 1999.

563 Garcia, S. L. M., Pandit, S., Navea, J. G., and Grassian, V. H.: Nitrous Acid (HONO)
564 Formation from the Irradiation of Aqueous Nitrate Solutions in the Presence of
565 Marine Chromophoric Dissolved Organic Matter: Comparison to Other Organic
566 Photosensitizers, *Acs Earth and Space Chemistry*, 5, 3056-3064,
567 10.1021/acsearthspacechem.1c00292, 2021.

568 George, C., Ammann, M., D'Anna, B., Donaldson, D. J., and Nizkorodov, S. A.:
569 Heterogeneous Photochemistry in the Atmosphere, *Chemical Reviews*, 115,
570 4218-4258, 10.1021/cr500648z, 2015.

571 Goodman, A. L., Bernard, E. T., and Grassian, V. H.: Spectroscopic study of nitric
572 acid and water adsorption on oxide particles: Enhanced nitric acid uptake kinetics in
573 the presence of adsorbed water, *Journal of Physical Chemistry A*, 105, 6443-6457,
574 10.1021/jp0037221, 2001.

575 Harris, G. W., Carter, W. P. L., Winer, A. M., Pitts, J. N., Platt, U., and Perner, D.:
576 Observations of nitrous-acid in the los-angeles atmosphere and implications for
577 predictions of ozone precursor relationships, *Environmental Science & Technology*,

578 16, 414-419, 10.1021/es00101a009, 1982.

579 Hot, J., Martinez, T., Wayser, B., Ringot, E., and Bertron, A.: Photocatalytic
580 degradation of NO/NO₂ gas injected into a 10 m³ experimental chamber,
581 Environmental Science and Pollution Research, 24, 12562-12570,
582 10.1007/s11356-016-7701-2, 2017.

583 Huang, L., Zhao, Y., Li, H., and Chen, Z.: Kinetics of Heterogeneous Reaction of
584 Sulfur Dioxide on Authentic Mineral Dust: Effects of Relative Humidity and
585 Hydrogen Peroxide, Environmental Science & Technology, 49, 10797-10805,
586 10.1021/acs.est.5b03930, 2015.

587 Jiyeon, Park, Myoseon, Jang, Zechen, and Yu: Heterogeneous Photo-oxidation of SO₂
588 in the Presence of Two Different Mineral Dust Particles: Gobi and Arizona Dust,
589 Environmental Science & Technology, 51, 9605-9613, 10.1021/acs.est.7b00588,
590 2017.

591 Kasibhatla, P., Sherwen, T., Evans, M. J., Carpenter, L. J., Reed, C., Alexander, B.,
592 Chen, Q., Sulprizio, M. P., Lee, J. D., Read, K. A., Bloss, W., Crilley, L. R., Keene, W.
593 C., Pszenny, A. A. P., and Hodzic, A.: Global impact of nitrate photolysis in sea-salt
594 aerosol on NO_x, OH, and O₃ in the marine boundary layer, Atmospheric Chemistry
595 and Physics, 18, 11185-11203, 10.5194/acp-18-11185-2018, 2018.

596 Kim, W.-H., Song, J.-M., Ko, H.-J., Kim, J. S., Lee, J. H., and Kang, C.-H.:
597 Comparison of Chemical Compositions of Size-segregated Atmospheric Aerosols
598 between Asian Dust and Non-Asian Dust Periods at Background Area of Korea,
599 Bulletin of the Korean Chemical Society, 33, 3651-3656,
600 10.5012/bkcs.2012.33.11.3651, 2012.

601 Lee, J. D., Moller, S. J., Read, K. A., Lewis, A. C., Mendes, L., and Carpenter, L. J.:
602 Year-round measurements of nitrogen oxides and ozone in the tropical North Atlantic
603 marine boundary layer, Journal of Geophysical Research-Atmospheres, 114, D21302,
604 10.1029/2009jd011878, 2009.

605 Lesko, D. M. B., Coddens, E. M., Swomley, H. D., Welch, R. M., Borgatta, J., and
606 Navea, J. G.: Photochemistry of nitrate chemisorbed on various metal oxide surfaces,
607 Physical Chemistry Chemical Physics, 17, 20775-20785, 10.1039/c5cp02903a, 2015.

608 Li, X., Rohrer, F., Brauers, T., Hofzumahaus, A., Lu, K., Shao, M., Zhang, Y. H., and
609 Wahner, A.: Modeling of HCHO and CHOCHO at a semi-rural site in southern China
610 during the PRIDE-PRD2006 campaign, *Atmospheric Chemistry and Physics*, 14,
611 12291-12305, 10.5194/acp-14-12291-2014, 2014.

612 Linsebigler, A. L., Lu, G. Q., and Yates, J. T.: Photocatalysis on TiO₂
613 surfaces-principles, mechanisms, and selected results, *Chemical Reviews*, 95,
614 735-758, 10.1021/cr00035a013, 1995.

615 Ma, Q., Zhong, C., Ma, J., Ye, C., Zhao, Y., Liu, Y., Zhang, P., Chen, T., Liu, C., Chu,
616 B., and He, H.: Comprehensive Study about the Photolysis of Nitrates on Mineral
617 Oxides, *Environmental Science & Technology*, 55, 8604-8612,
618 10.1021/acs.est.1c02182, 2021.

619 Maeda, N., Urakawa, A., Sharma, R., and Baiker, A.: Influence of Ba precursor on
620 structural and catalytic properties of Pt-Ba/alumina NO_x storage-reduction catalyst,
621 *Applied Catalysis B-Environmental*, 103, 154-162, 10.1016/j.apcatb.2011.01.022,
622 2011.

623 Monge, M. E., D'Anna, B., and George, C.: Nitrogen dioxide removal and nitrous
624 acid formation on titanium oxide surfaces--an air quality remediation process?,
625 *Physical Chemistry Chemical Physics*, 12, 8991-8998, 10.1039/b925785c, 2010.

626 Ndour, M., Conchon, P., D'Anna, B., Ka, O., and George, C.: Photochemistry of
627 mineral dust surface as a potential atmospheric renoxification process, *Geophysical
628 Research Letters*, 36, 4, 10.1029/2008gl036662, 2009.

629 Ninneman, M., Lu, S., Zhou, X. L., and Schwab, J.: On the Importance of
630 Surface-Enhanced Renoxification as an Oxides of Nitrogen Source in Rural and
631 Urban New York State, *Acs Earth and Space Chemistry*, 4, 1985-1992,
632 10.1021/acsearthspacechem.0c00185, 2020.

633 Ostaszewski, C. J., Stuart, N. M., Lesko, D. M. B., Kim, D., Lueckheide, M. J., and
634 Navea, J. G.: Effects of Coadsorbed Water on the Heterogeneous Photochemistry of
635 Nitrates Adsorbed on TiO₂, *Journal of Physical Chemistry A*, 122, 6360-6371,
636 10.1021/acs.jpca.8b04979, 2018.

637 Pandit, S., Garcia, S. L. M., and Grassian, V. H.: HONO Production from Gypsum

638 Surfaces Following Exposure to NO₂ and HNO₃: Roles of Relative Humidity and
639 Light Source, *Environmental Science & Technology*, 55, 9761-9772,
640 10.1021/acs.est.1c01359, 2021.

641 Platt, U., Perner, D., Harris, G. W., Winer, A. M., and Pitts, J. N.: Observations of
642 nitrous-acid in an urban atmosphere by differential optical-absorption, *Nature*, 285,
643 312-314, 10.1038/285312a0, 1980.

644 Read, K. A., Mahajan, A. S., Carpenter, L. J., Evans, M. J., Faria, B. V. E., Heard, D.
645 E., Hopkins, J. R., Lee, J. D., Moller, S. J., Lewis, A. C., Mendes, L., McQuaid, J. B.,
646 Oetjen, H., Saiz-Lopez, A., Pilling, M. J., and Plane, J. M. C.: Extensive
647 halogen-mediated ozone destruction over the tropical Atlantic Ocean, *Nature*, 453,
648 1232-1235, 10.1038/nature07035, 2008.

649 Reed, C., Evans, M. J., Crilley, L. R., Bloss, W. J., Sherwen, T., Read, K. A., Lee, J.
650 D., and Carpenter, L. J.: Evidence for renoxification in the tropical marine boundary
651 layer, *Atmospheric Chemistry and Physics*, 17, 4081-4092,
652 10.5194/acp-17-4081-2017, 2017.

653 Romer, P. S., Wooldridge, P. J., Crouse, J. D., Kim, M. J., Wennberg, P. O., Dibb, J.
654 E., Scheuer, E., Blake, D. R., Meinardi, S., Brosius, A. L., Thames, A. B., Miller, D.
655 O., Brune, W. H., Hall, S. R., Ryerson, T. B., and Cohen, R. C.: Constraints on
656 Aerosol Nitrate Photolysis as a Potential Source of HONO and NO_x, *Environmental
657 Science & Technology*, 52, 13738-13746, 10.1021/acs.est.8b03861, 2018.

658 Rosseler, O., Sleiman, M., Nahuel Montesinos, V., Shavorskiy, A., Keller, V., Keller,
659 N., Litter, M. I., Bluhm, H., Salmeron, M., and Destailats, H.: Chemistry of NO_x on
660 TiO₂ Surfaces Studied by Ambient Pressure XPS: Products, Effect of UV Irradiation,
661 Water, and Coadsorbed K⁺, *Journal of Physical Chemistry Letters*, 4, 536-541,
662 10.1021/jz302119g, 2013.

663 Schuttlefield, J., Rubasinghege, G., El-Maazawi, M., Bone, J., and Grassian, V. H.:
664 Photochemistry of adsorbed nitrate, *Journal of the American Chemical Society*, 130,
665 12210-12211, 10.1021/ja802342m, 2008.

666 Schutze, M. and Herrmann, H.: Uptake of the NO₃ radical on aqueous surfaces,
667 *Journal of Atmospheric Chemistry*, 52, 1-18, 10.1007/s10874-005-6153-8, 2005.

668 Schwartz-Narbonne, H., Jones, S. H., and Donaldson, D. J.: Indoor Lighting Releases
669 Gas Phase Nitrogen Oxides from Indoor Painted Surfaces, *Environmental Science &*
670 *Technology Letters*, 6, 92-97, 10.1021/acs.estlett.8b00685, 2019.

671 Seltzer, K. M., Vizuete, W., and Henderson, B. H.: Evaluation of updated nitric acid
672 chemistry on ozone precursors and radiative effects, *Atmospheric Chemistry and*
673 *Physics*, 15, 5973-5986, 10.5194/acp-15-5973-2015, 2015.

674 Shang, J., Xu, W. W., Ye, C. X., George, C., and Zhu, T.: Synergistic effect of
675 nitrate-doped TiO₂ aerosols on the fast photochemical oxidation of formaldehyde,
676 *Scientific Reports*, 7, 1161, 10.1038/s41598-017-01396-x, 2017.

677 Shi, Q., Tao, Y., Krechmer, J. E., Heald, C. L., Murphy, J. G., Kroll, J. H., and Ye, Q.:
678 Laboratory Investigation of Renoxification from the Photolysis of Inorganic
679 Particulate Nitrate, *Environmental science & technology*, 55, 854-861,
680 10.1021/acs.est.0c06049, 2021.

681 Stemmler, K., Ammann, M., Donders, C., Kleffmann, J., and George, C.:
682 Photosensitized reduction of nitrogen dioxide on humic acid as a source of nitrous
683 acid, *Nature*, 440, 195-198, 10.1038/nature04603, 2006.

684 Sun, Y. L., Zhuang, G. S., Wang, Y., Zhao, X. J., Li, J., Wang, Z. F., and An, Z. S.:
685 Chemical composition of dust storms in Beijing and implications for the mixing of
686 mineral aerosol with pollution aerosol on the pathway, *Journal of Geophysical*
687 *Research-Atmospheres*, 110, D24209, 10.1029/2005jd006054, 2005.

688 Tang, M., Liu, Y., He, J., Wang, Z., Wu, Z., and Ji, D.: In situ continuous hourly
689 observations of wintertime nitrate, sulfate and ammonium in a megacity in the North
690 China plain from 2014 to 2019: Temporal variation, chemical formation and regional
691 transport, *Chemosphere*, 262, 10.1016/j.chemosphere.2020.127745, 2021.

692 Tian, S. S., Liu, Y. Y., Wang, J., Wang, J., Hou, L. J., Lv, B., Wang, X. H., Zhao, X. Y.,
693 Yang, W., Geng, C. M., Han, B., and Bai, Z. P.: Chemical Compositions and Source
694 Analysis of PM_{2.5} during Autumn and Winter in a Heavily Polluted City in China,
695 *Atmosphere*, 11, 19, 10.3390/atmos11040336, 2020.

696 Verbruggen, S. W.: TiO₂ photocatalysis for the degradation of pollutants in gas phase:
697 From morphological design to plasmonic enhancement, *Journal of Photochemistry*

698 and Photobiology C-Photochemistry Reviews, 24, 64-82,
699 10.1016/j.jphotochemrev.2015.07.001, 2015.

700 Wang, H., Miao, Q., Shen, L., Yang, Q., Wu, Y., Wei, H., Yin, Y., Zhao, T., Zhu, B.,
701 and Lu, W.: Characterization of the aerosol chemical composition during the
702 COVID-19 lockdown period in Suzhou in the Yangtze River Delta, China, Journal of
703 environmental sciences (China), 102, 110-122, 10.1016/j.jes.2020.09.019, 2021.

704 Wayne, R. P., Barnes, I., Biggs, P., Burrows, J. P., Canosamas, C. E., Hjorth, J., Lebras,
705 G., Moortgat, G. K., Perner, D., Poulet, G., Restelli, G., and Sidebottom, H.: The
706 nitrate radical-physics, chemistry, and the atmosphere, Atmospheric Environment Part
707 a-General Topics, 25, 1-203, 10.1016/0960-1686(91)90192-a, 1991.

708 Ye, C., Gao, H., Zhang, N., and Zhou, X.: Photolysis of Nitric Acid and Nitrate on
709 Natural and Artificial Surfaces, Environmental Science & Technology, 50, 3530-3536,
710 10.1021/acs.est.5b05032, 2016a.

711 Ye, C., Zhang, N., Gao, H., and Zhou, X.: Photolysis of Particulate Nitrate as a Source
712 of HONO and NO_x, Environmental Science & Technology, 51, 6849-6856,
713 10.1021/acs.est.7b00387, 2017.

714 Ye, C., Zhou, X., Pu, D., Stutz, J., Festa, J., Spolaor, M., Tsai, C., Cantrell, C.,
715 Mauldin, R. L., III, Campos, T., Weinheimer, A., Hornbrook, R. S., Apel, E. C.,
716 Guenther, A., Kaser, L., Yuan, B., Karl, T., Haggerty, J., Hall, S., Ullmann, K., Smith,
717 J. N., Ortega, J., and Knote, C.: Rapid cycling of reactive nitrogen in the marine
718 boundary layer, Nature, 532, 489-491, 10.1038/nature17195, 2016b.

719 Zhou, J. B., Xing, Z. Y., Deng, J. J., and Du, K.: Characterizing and sourcing ambient
720 PM_{2.5} over key emission regions in China I: Water-soluble ions and carbonaceous
721 fractions, Atmospheric Environment, 135, 20-30, 10.1016/j.atmosenv.2016.03.054,
722 2016.

723 Zhou, X. L., Gao, H. L., He, Y., Huang, G., Bertman, S. B., Civerolo, K., and Schwab,
724 J.: Nitric acid photolysis on surfaces in low-NO_x environments: Significant
725 atmospheric implications, Geophysical Research Letters, 30, 2217,
726 10.1029/2003gl018620, 2003.

727